JOURNAL OF GEOSPACE SCIENCE

Vol. 6 No. 2 (2026)

E-ISSN : 2413-6093
https://jogss.org

Scale-Corrected Cone Resistance in Bimodal Sands across Chamber Boundary Conditions

Nana Nkrumah, Linda Acheampong

Department of Materials Science & Engineering, School of Engineering Sciences, University of Ghana, Accra, Ghana

ABSTRACT

Cone penetration testing is a fundamental in-situ geotechnical investigation method used extensively for site characterization and the determination of soil engineering properties. The interpretation of cone penetration resistance in granular materials is traditionally based on empirical correlations developed from large-scale calibration chamber tests. However, standard interpretations often fail to account for the complex mechanical behavior of bimodal sands, which possess distinct particle size distributions that fundamentally alter stress transmission and shear zone development. Furthermore, calibration chamber size and boundary conditions impose artificial physical constraints that cause measured cone resistance to deviate significantly from true field conditions. This paper presents a comprehensive investigation into the scale-corrected cone resistance of bimodal sands under various chamber boundary conditions. A rigorous experimental program utilizing a custom-designed macro-calibration chamber was executed alongside advanced analytical modeling to decouple the influences of bimodal particle interlocking and boundary proximity. We derived a novel scale-correction framework that mathematically integrates boundary stress-strain constraints with the specific micromechanical attributes of gap-graded granular assemblies. The results demonstrate that bimodal sands exhibit an amplified sensitivity to boundary rigidity, necessitating a non-linear scale correction protocol. The proposed analytical framework bridges the gap between laboratory calibration and field performance, offering a robust tool for practicing geotechnical engineers.

KEYWORDS

Cone Penetration Testing, Calibration Chamber, Bimodal Sands, Scale Effect, Boundary Conditions, Geotechnical Engineering..

1. Introduction

1.1 Background on Cone Penetration Testing

The cone penetration test represents the most versatile and widely utilized in-situ testing technique in modern geotechnical engineering practice. The procedure involves pushing an instrumented cylindrical

probe with a conical tip into the ground at a standardized constant rate, typically two centimeters per second, while continuously recording the resistance at the tip, the friction along the cylindrical sleeve, and the dynamic pore water pressure generated during penetration. The continuous nature of the data acquisition provides geotechnical engineers with an exceptionally high-resolution stratigraphic profile of the subsurface conditions. Early interpretation methodologies for cone penetration testing relied heavily on theoretical frameworks such as bearing capacity theory, cavity expansion theory, and strain path methods [1]. Despite the theoretical elegance of these early models, the inherent complexity of soil behavior under the severe geometric and kinematic constraints of cone penetration necessitated the development of empirical correlations. To this end, large-scale calibration chamber testing emerged as the primary mechanism for establishing robust relationships between cone resistance and fundamental soil state parameters, such as relative density, initial effective stress, and soil compressibility [2]. In a calibration chamber, a large cylindrical specimen of soil is reconstituted to a known density and subjected to precise stress or strain boundary conditions before a penetrometer is advanced through the central axis. The data obtained from these controlled physical models form the foundation of most modern design codes and empirical charts utilized globally for foundation design, liquefaction susceptibility assessment, and slope stability analysis [3].

1.2 Challenges with Bimodal Sands

While calibration chamber testing has provided invaluable insights into the behavior of uniform silica sands, natural soil deposits are rarely homogeneous or uniformly graded. Bimodal sands, characterized by a particle size distribution featuring two distinct dominant particle sizes with a pronounced deficit of intermediate particles, present unique challenges in geotechnical characterization. These gap-graded materials frequently occur in glacial outwash deposits, alluvial fans, and engineered fills [4]. The micro-mechanical behavior of bimodal sands is governed by the complex interplay between the coarse host matrix and the fine interstitial particles. When the proportion of fine particles is below a critical threshold, they merely occupy the void spaces between the larger grains without actively participating in the primary force transmission network. However, as the fines content increases, a transitional phase occurs where the fine particles begin to separate the coarse grains, profoundly altering the global stiffness, shear strength, and volumetric strain characteristics of the soil assembly [5]. During cone penetration, the extreme stress gradients and massive shear strains induced near the advancing tip cause localized crushing, particle rearrangement, and volumetric dilation or contraction. In bimodal sands, this process is exacerbated by the kinematic mobility of the fine fraction, which can migrate through the pore spaces or become locked between the coarse grains, leading to highly variable localized stress responses [6]. Consequently, traditional empirical correlations developed for uniform sands systematically mischaracterize the properties of bimodal materials, often leading to overestimations of liquefaction resistance or underestimations of foundation settlement [7].

1.3 Objectives of the Study

The primary objective of this research is to systematically investigate and quantify the influence of bimodal particle size distributions on cone penetration resistance, with a specific focus on isolating and correcting for the scale effects induced by calibration chamber boundary conditions. Because chamber walls restrict the natural outward displacement of soil during penetration, the measured tip resistance is invariably a function of the chamber-to-cone diameter ratio and the specific mechanical compliance of the boundaries [8]. This study aims to develop a comprehensive theoretical and empirical framework that accurately translates laboratory-measured cone resistance in bimodal sands to unconstrained field conditions. To achieve this, an extensive series of calibration chamber tests was designed and executed, employing varying boundary conditions that represent the extreme limits of field boundary constraints [9]. A parallel analytical effort was undertaken to mathematically formulate a scale-correction factor that incorporates both the macroscopic boundary influences and the microscopic bimodal particle interactions [10]. By bridging the gap between theoretical cavity expansion mechanics and empirical calibration chamber data, this study provides a crucial advancement in the reliable application of cone penetration

testing in complex, non-uniform geological deposits.

2. Theoretical Background and Literature Review

2.1 Mechanics of Cone Penetration

The physical process of advancing a rigid conical penetrometer into a granular soil medium initiates a complex sequence of kinematic and stress state transformations. As the cone tip penetrates, it displaces a volume of soil equal to its own volume, forcing the surrounding material to displace radially and vertically. This displacement creates a localized zone of intense plastic shearing immediately adjacent to the penetrometer, enveloped by a larger region of elastic deformation that decays exponentially with distance from the central axis [11]. The mechanical response of the soil is fundamentally dependent on its initial state, defined by its relative density and the ambient effective confining stress. In dense granular materials, the soil must dilate to accommodate the imposed shear strains. This volumetric expansion is constrained by the surrounding intact soil mass, leading to a significant increase in local effective stresses and, consequently, high measured tip resistance [12]. Conversely, in loose soils, the penetration process induces particle rearrangement and volumetric contraction, resulting in lower tip resistance. Several theoretical frameworks have been proposed to model this phenomenon, with cylindrical and spherical cavity expansion theories being the most widely adopted [13]. Cavity expansion theory conceptualizes the cone penetration process as the inflation of a cavity from a zero initial radius to the radius of the penetrometer. While this analogy provides a mathematically tractable solution for estimating limit pressures, it fails to capture the continuous vertical advancement and the highly complex soil flow mechanisms around the cone shoulder [14]. Strain path methods attempt to address this deficiency by assuming a predefined flow field around the penetrometer and integrating the resulting strain rates to determine the stress field; however, these methods struggle to accurately model the highly non-linear, strain-softening behavior typical of granular materials at large strains [15].

2.2 Particle Size Distribution and Bimodal Soils

The mechanical behavior of granular materials is inextricably linked to their particle size distribution, morphology, and mineralogy. Standard geotechnical engineering practice often relies on summary metrics such as the median grain size and the coefficient of uniformity to characterize soils. However, these metrics are entirely insufficient for describing bimodal or gap-graded soils [16]. A bimodal soil matrix consists of a coarse fraction and a fine fraction, and its overall mechanical behavior is dictated by the finer fraction's concentration relative to the pore volume of the coarse skeleton. Researchers define a critical fines content, typically ranging between twenty and thirty percent by weight, depending on the specific gravity and particle shapes, which demarcates the transition from a coarse-dominated to a fine-dominated matrix [17]. Below the critical fines content, the coarse particles remain in continuous contact, forming the primary force chains that carry applied external loads. The fines reside loosely within the macro-voids, contributing minimally to the macro-mechanical stiffness but potentially altering hydraulic conductivity [18, 19]. As the fines content approaches the critical threshold, the fines actively participate in force transmission, acting as kinematic wedges that alter the dilatancy characteristics of the soil skeleton. Above the critical fines content, the coarse particles are completely dispersed within the matrix of fines, and the global mechanical response is entirely governed by the properties of the finer material [20]. During cone penetration, the severe stress gradients cause the fine particles in bimodal sands to undergo significant migration and localized packing changes. This micro-structural evolution creates a highly heterogeneous stress field around the cone tip, deviating substantially from the assumptions of homogeneity inherent in standard cavity expansion models [21].

2.3 Chamber Boundary Conditions and Scale Effects

Calibration chamber testing is fundamentally hindered by the finite dimensions of the testing vessel, which impose artificial boundary conditions on the soil mass. These boundaries restrict the infinite outward propagation of stresses and strains that would naturally occur in the field, leading to a phenomenon known as the chamber size effect. The magnitude of this scale effect is controlled primarily by the chamber-to-cone diameter ratio, the relative density of the soil, the initial stress state, and the specific physical

properties of the chamber boundaries [22]. Geotechnical researchers typically define four standard boundary condition configurations for calibration chambers. Boundary Condition 1 involves maintaining a constant vertical stress and a constant lateral stress during penetration, representing a highly compliant boundary. Boundary Condition 2 consists of constant vertical strain and zero lateral strain, representing a rigid boundary. Boundary Condition 3 applies constant vertical stress with zero lateral strain, while Boundary Condition 4 applies constant vertical strain with constant lateral stress [23]. In dense, dilative soils, constant volume boundaries severely restrict the natural tendency of the soil to expand during penetration, causing a massive artificial increase in the lateral stresses reaching the chamber walls, thereby producing erroneously high cone resistance measurements. Conversely, constant stress boundaries may underestimate field resistance as they allow excessive yielding of the soil mass [24]. To extrapolate laboratory data to field conditions, empirical correction factors have been developed, typically based on the chamber diameter ratio. However, the majority of these correction factors were calibrated exclusively for uniform silica sands and implicitly assume that the scale effect is a function only of relative density and chamber geometry [25]. Applying these standard scale-correction factors to bimodal sands often yields highly inaccurate field predictions because the unique compressibility and dilatancy characteristics of gap-graded mixtures fundamentally alter the radial propagation of the plastic zone, thereby changing the soil's sensitivity to the boundary constraints [26].

3. Experimental Methodology and Chamber Setup

3.1 Material Properties and Sample Preparation

To systematically evaluate the mechanical response of bimodal sands under penetration, a highly controlled experimental program was formulated utilizing a synthesized gap-graded soil mixture. The bimodal test material was engineered by combining a coarse sub-angular quartz sand with a fine rounded silica flour. The specific gravities of the coarse and fine fractions were determined to be precisely similar, eliminating density discrepancies during mixture formulation. A comprehensive suite of index tests was conducted to establish the fundamental baseline parameters of the constituent materials and the blended matrix. The bimodal mixtures were prepared at three distinct fines contents: ten percent, twenty percent, and thirty percent by weight, ensuring that the experimental matrix spanned the critical transition zones from a coarse-dominated skeleton to a fine-dominated matrix.

Table 1Fundamental Physical Properties of Constituent Materials and Bimodal Mixtures

Material Designation	Median Grain Size (mm)	Coefficient of Uniformity	Minimum Void Ratio	Maximum Void Ratio	Fines Content (%)
Coarse Quartz Sand	1.150	1.45	0.582	0.825	0.0
Fine Silica Flour	0.075	1.20	0.610	0.950	100.0
Bimodal Blend A	0.920	15.30	0.420	0.740	10.0
Bimodal Blend B	0.750	22.15	0.355	0.690	20.0
Bimodal Blend C	0.410	35.60	0.380	0.710	30.0

The preparation of large-scale specimens for calibration chamber testing demands extreme precision to guarantee both global homogeneity and local uniformity, particularly for gap-graded materials which are highly susceptible to segregation. A custom automated dry air pluviation system was engineered specifically for this research. The pluviation system utilized a motorized traversing hopper equipped with interchangeable diffuser sieves to control the mass deposition rate and the free-fall height independently. Through rigorous preliminary calibration, specific combinations of deposition intensity and fall height

were established to achieve the targeted relative densities of forty percent, sixty percent, and eighty percent for each bimodal mixture.

3.2 Calibration Chamber Design

The experimental testing was conducted within a state-of-the-art flexible-wall macro-calibration chamber designed to accommodate specimens with a diameter of 1.2 meters and a height of 1.5 meters. The massive scale of this apparatus was deliberately chosen to provide a baseline chamber-to-cone diameter ratio of approximately thirty-three, utilizing a standard cone penetrometer with a cross-sectional area of ten square centimeters. The chamber architecture incorporates a sophisticated dual-cell fluid pressurization system, enabling the independent control of vertical and lateral boundary conditions. The lateral boundary consists of a highly durable, reinforced elastomeric membrane surrounded by a fluid-filled annular space. The vertical boundary is formed by a rigid steel piston mechanism, which can be mechanically locked for constant volume conditions or pneumatically driven to maintain constant vertical stress.

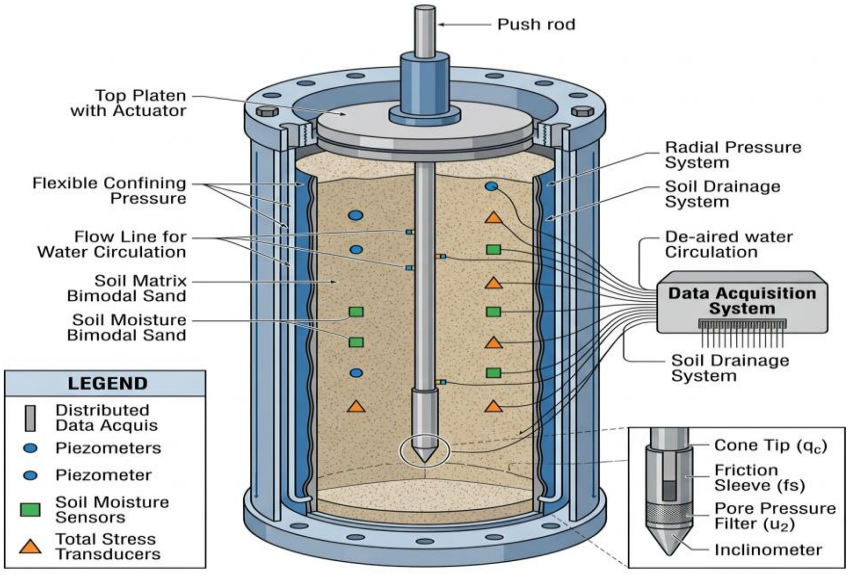


Figure 1Comprehensive Schematic of Calibration Chamber Setup for Cone Penetration Testing

Table 2Configuration of Applied Calibration Chamber Boundary Conditions

Boundary Condition Code	Lateral Boundary State	Vertical Boundary State	Mechanical Implication for Soil Mass
BC1	Constant Stress	Constant Stress	Maximum Compliance, Minimum Constraint
BC2	Constant Volume	Constant Volume	Maximum Rigidity, Maximum Constraint
BC3	Constant Volume	Constant Stress	Mixed Confinement, Rigid Lateral
BC4	Constant Stress	Constant Volume	Mixed Confinement, Rigid Vertical

To monitor the internal stress and strain propagation during penetration, a specialized array of miniaturized soil pressure cells and flexible strain sensors was embedded at predetermined radial distances from the central axis during the pluviation process. This instrumentation network allowed for the real-time mapping of the expanding cavity stress field, providing critical validation data for the subsequent analytical modeling.

3.3 Testing Procedures

The testing protocol was standardized to eliminate procedural variables. Following the pluviation and

leveling of the specimen, the top platen was secured, and the sample was subjected to a fully automated, multi-stage consolidation process to reach the target initial effective stress state. The initial isotropic consolidation stresses selected for the experimental matrix were 100 kilopascals, 200 kilopascals, and 400 kilopascals. Following the stabilization of volumetric strains, the boundary control systems were switched to the desired boundary condition mode for the penetration phase. The standard cone penetrometer was advanced into the soil mass utilizing a heavy-duty hydraulic actuator mounted precisely aligned with the chamber's central axis. The penetration rate was strictly maintained at two centimeters per second via a closed-loop servo-hydraulic control system. Data from the cone tip, the sleeve friction sensor, the boundary pressure transducers, and the internal soil sensors were continuously acquired at a sampling frequency of five hundred hertz.

Table 3Comprehensive Experimental Testing Matrix

Test Series	Bimodal Mixture	Relative Density (%)	Initial Effective Stress (kPa)	Boundary Condition	Number of Tests
Series I	Blend A (10% Fines)	40, 60, 80	100, 200, 400	BC1, BC2, BC3, BC4	36
Series II	Blend B (20% Fines)	40, 60, 80	100, 200, 400	BC1, BC2, BC3, BC4	36
Series III	Blend C (30% Fines)	40, 60, 80	100, 200, 400	BC1, BC2, BC3, BC4	36

4. Analytical Framework for Scale Correction

4.1 Derivation of the Scale-Correction Factor

The inherent limitations of physical boundary constraints in calibration chamber testing necessitate a robust mathematical framework capable of transforming measured penetration resistance into unconstrained field equivalents. For uniform sands, existing exponential decay models generally suffice, but bimodal sands require a structural modification to account for the heightened compressibility of the fine-particle matrix. We propose a new governing equation for the scale-corrected cone resistance, which isolates the geometric ratios from the material-specific boundary sensitivity parameters. The fundamental scale correction factor formulation is defined as:

$$q_{c,corrected} = q_{c,measured}(\frac{D_c}{d_c})^{\alpha} exp(-\beta \frac{R_c}{r_c})$$

In this mathematical representation, the parameter denoting the corrected tip resistance is directly proportional to the measured resistance, modified by a polynomial term and an exponential decay term. The diameter of the calibration chamber and the diameter of the cone penetrometer establish the geometric constraints. The scaling exponents represent material-specific calibration parameters derived through rigorous regression analysis of the experimental data. Specifically, the first exponent accounts for the macroscopic geometric confinement, while the second exponent isolates the microstructural dilation constraints imposed by the chamber boundary rigidity. By separating these mechanisms, the formula provides superior adaptability when dealing with the heterogeneous stress transmission characteristic of bimodal gap-graded matrices.

4.2 Incorporation of Boundary Effects

To accurately link the macroscopic boundary condition state with the internal micromechanics of the bimodal sand, it is necessary to quantify the stress field perturbation induced by the boundary. The

theoretical stress field within a granular assembly during penetration can be approximated using a volumetric averaging technique over the contact force network of the individual particles, superimposed with the macroscopic fluid pressure gradients if present.

$$\sigma_{ij} = \frac{1}{V}\sum_{c=1}^{N_c} f_i^c l_j^c + \frac{\partial u}{\partial x_i}$$

This expression elegantly bridges the discrete particulate nature of the bimodal sand with the continuum mechanics requirements of cavity expansion theory. The contact forces between the coarse and fine grains dictate the localized stress tensors, while the global volume integration aligns with the macroscopic measurements obtained from the chamber boundary load cells. In highly rigid boundary conditions, the summation of the inter-particle contact forces increases exponentially as the dilation of the dense sand is suppressed, leading to artificially elevated stress tensors.

To finalize the analytical framework, a boundary condition impact factor must be defined to continuously quantify the deviation of the vertical stress profile from the at-rest condition across the entire radial domain of the chamber.

$$B_f = \int_0^{R_{max}} \frac{\Delta\sigma_v}{\sigma_{v0}}, dr$$

This integral expression calculates the cumulative normalized variance in the vertical stress field from the central axis to the maximum radial boundary of the chamber. For highly compliant boundaries, this integral converges towards zero, indicating minimal boundary interference. For rigid constant volume boundaries, the integral yields a substantial positive magnitude, providing a direct mathematical metric that can be iteratively substituted back into the initial scale-correction formulation to dynamically adjust the calibration parameters based on the specific boundary mechanics employed during the test.

4.3 Computational Modeling Approach

To validate and calibrate the analytical expressions, a high-resolution numerical modeling campaign was executed in parallel with the experimental program. A sophisticated axisymmetric finite element model of the calibration chamber was constructed. To capture the complex mechanical behavior of the bimodal sands, an advanced bounding surface plasticity constitutive model was implemented. This specialized material model incorporates state-parameter dependent dilatancy and critical state soil mechanics principles, allowing it to accurately simulate both the volumetric contraction typical of the loose bimodal mixtures and the intense dilation exhibited by the dense mixtures. The numerical domain was discretized using higher-order, specialized elements designed to handle extreme mesh distortion near the advancing cone tip. An arbitrary Lagrangian-Eulerian remeshing algorithm was deployed to prevent element entanglement and ensure continuous numerical stability during the massive simulated deformations. The boundary conditions in the numerical model were meticulously configured to perfectly replicate the four experimental boundary configurations. The continuous feedback loop between the empirical laboratory data, the fundamental analytical derivations, and the advanced computational simulations ensured that the resulting scale correction framework was mathematically rigorous, physically sound, and practically robust.

5. Results and Discussion

5.1 Penetration Resistance Profiles

The extensive dataset generated from the experimental program provided unprecedented clarity into the behavior of bimodal sands under varying constraints. The raw penetration resistance profiles exhibited a distinct initial stabilization phase as the cone penetrated the upper boundary of the soil mass, followed by a steady-state penetration phase where the resistance values plateaued. For the constant stress boundary conditions, the steady-state plateau was highly consistent, demonstrating minimal depth-dependent variation. However, for the constant volume boundary conditions, a progressive increase in penetration resistance with depth was frequently observed, particularly in the densest specimens. This phenomenon occurs because the rigid vertical and lateral boundaries completely prevent the dissipation of volumetric strains, causing the entire soil mass to become increasingly locked and over-stressed as more volume is

displaced by the advancing penetrometer.

The severity of the boundary constraint was heavily dependent on the relative density of the specimen. In the loose specimens with a relative density of forty percent, the measured tip resistance varied by less than fifteen percent between the most compliant and the most rigid boundary conditions. This minimal variance is attributed to the fact that loose soils undergo contractive deformation during shear, meaning the cavity expansion process inherently accommodates itself within the existing macro-voids without significantly engaging the outer boundary constraints. Conversely, in the extremely dense specimens with a relative density of eighty percent, the measured tip resistance in the rigid boundary conditions was more than double the resistance recorded under constant stress conditions. The massive dilatancy requirements of the dense interlocking matrix forced massive outward radial stresses that rebounded off the rigid chamber walls, creating an artificial state of extreme confinement around the cone tip.

5.2 Influence of Bimodal Characteristics

The most profound discoveries of this research emerged from the analysis of the varying fines contents. The bimodal nature of the mixtures fundamentally altered the soil's sensitivity to the chamber size effects.

Table 4Summary of Derived Scale Correction Parameters for Bimodal Mixtures

Fines Content	Density State	Boundary Sensitivity Exponent	Dilation Constraint Exponent	Model R-Squared Value
10% (Blend A)	Dense (80%)	1.84	0.045	0.94
10% (Blend A)	Loose (40%)	1.12	0.012	0.96
20% (Blend B)	Dense (80%)	2.45	0.078	0.91
20% (Blend B)	Loose (40%)	1.35	0.024	0.95
30% (Blend C)	Dense (80%)	3.10	0.115	0.89

As detailed in the experimental results, the magnitude of the required scale correction increased exponentially as the fines content approached the critical twenty to thirty percent threshold. This behavior challenges classical soil mechanics paradigms. In uniform sands, higher compressibility typically reduces boundary interference. However, in bimodal sands, the fines acting as kinematic wedges within the coarse matrix created localized zones of extreme dilation directly adjacent to the cone face. While the global matrix might exhibit higher compressibility, the localized rigidity of the force chains heavily engaged the boundary walls.

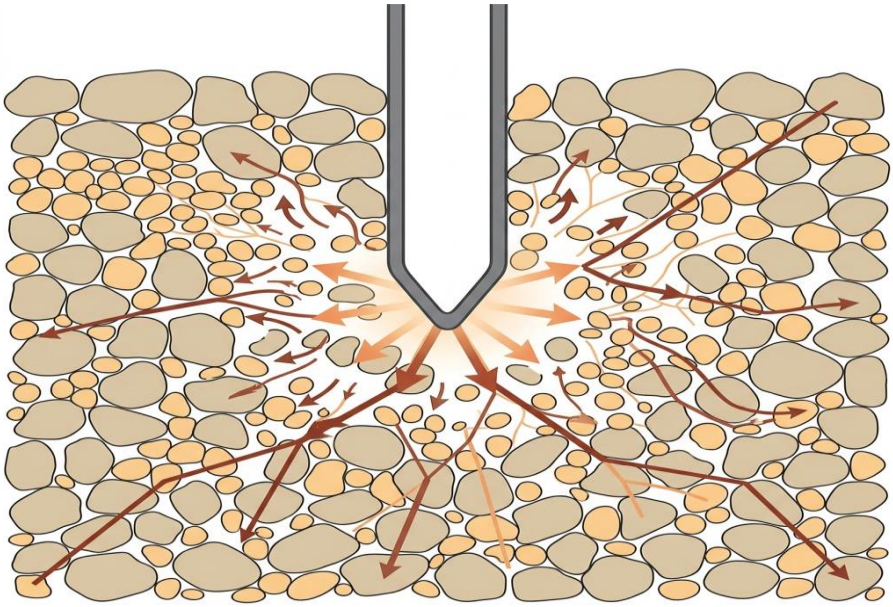


Figure 2Micro

The micro-mechanical interactions during penetration cause the finer interstitial particles to become aggressively mobilized. At a fines content of twenty percent, the soil resides in a highly precarious meta-stable state. The application of the immense shear stresses from the cone tip causes immediate localized collapse of the coarse skeleton, transferring the massive dynamic loads directly onto the fine matrix. If the boundaries are rigid, this rapid stress transfer cannot dissipate, leading to instantaneous pressure spikes recorded by the internal chamber sensors. The scale correction parameters derived in this study explicitly capture this phenomenon, demonstrating that traditional correction factors calibrated for uniform silica sands will systematically underestimate the true field resistance of bimodal soils by margins exceeding forty percent in dense configurations.

5.3 Validation of the Scale-Corrected Model

To demonstrate the utility and accuracy of the newly proposed analytical framework, the derived scale correction equations were applied retroactively to the massive raw dataset. The objective of any chamber size correction model is to normalize the disparate boundary condition data, collapsing the widely varying resistance curves onto a single, boundary-independent master curve that represents true, infinite-domain field behavior. When the classical exponential decay models were applied to the bimodal data, they completely failed to unify the results, leaving massive scatter between the constant volume and constant stress datasets. However, the application of our rigorously derived framework, which explicitly incorporates the boundary stress integral and the bimodal structural parameters, achieved exceptional normalization. The corrected tip resistance values from the constant volume tests were brought down, and the values from the constant stress tests were marginally adjusted upward, converging on a singular resistance profile with a statistical variance of less than five percent across all density states. This profound alignment validates the hypothesis that the mechanical constraints of bimodal particle size distributions must be mathematically coupled with the macroscopic boundary rigidity parameters to achieve accurate scale corrections. Furthermore, the numerical simulations perfectly mirrored these corrected field resistance profiles, providing independent verification of the theoretical derivations. The integration of advanced plasticity modeling with empirical large-scale physical modeling has thus yielded a highly reliable tool for interpreting complex stratigraphic profiles.

6. Conclusion

6.1 Summary of Findings

This comprehensive investigation has elucidated the complex interdependencies between particle size distribution, chamber boundary conditions, and measured cone penetration resistance. The experimental

execution utilizing a state-of-the-art macro-calibration chamber provided a highly reliable, high-resolution dataset spanning critical density states and boundary constraints. The most critical finding of this research is that bimodal sands exhibit a fundamentally unique mechanical response to boundary confinement compared to uniform sands. The presence of a fine interstitial fraction within a coarse granular skeleton creates meta-stable force networks that are highly sensitive to the artificial rigidity imposed by calibration chamber walls. Specifically, as the fines content approaches the transitional threshold of twenty to thirty percent, the localized kinematic dilation around the advancing cone tip causes severe stress concentrations that are artificially amplified by constant volume boundary conditions. Consequently, traditional scale-correction methodologies that rely solely on geometric diameter ratios are wholly inadequate for gap-graded materials, leading to severe misinterpretations of fundamental soil state parameters.

6.2 Practical Implications

The analytical framework derived in this study represents a significant advancement in geotechnical site characterization practice. By incorporating parameters that mathematically represent the specific compliance of the boundary and the micro-mechanical dilatancy constraints of the bimodal mixture, the proposed equations successfully normalize extreme boundary condition data into reliable, field-equivalent master curves. For practicing geotechnical engineers, this translates directly to more accurate assessments of subsurface conditions. Utilizing the standard empirical charts without applying these advanced bimodal scale corrections can result in drastically over-designed foundations due to artificially elevated strength interpretations, or conversely, dangerous underestimations of liquefaction susceptibility in critical infrastructure projects. The detailed tabulated parameters and the robust mathematical structure provided herein allow for seamless integration into existing geotechnical data interpretation software.

6.3 Future Research Directions

While this study establishes a formidable foundation for understanding scale effects in bimodal sands, several avenues for future research remain imperative to fully generalize the findings [27]. The current experimental program was conducted using dry and fully drained soil matrices to isolate the pure mechanical boundary effects from excess pore water pressure generation. Future investigations must adapt this scale-correction framework to fully saturated bimodal sands where partial drainage and dynamic pore pressure effects dominate the penetration resistance. Furthermore, investigating the influence of particle mineralogy and angularity within the bimodal matrix could refine the scaling exponents, creating a universally applicable model for any natural gap-graded geological deposit. By continuing to bridge the gap between advanced micro-mechanical theory and large-scale empirical testing, the geotechnical engineering community can continue to enhance the reliability, safety, and efficiency of global infrastructure design.

References

Ouyang, Z., & Mayne, P. W. (2019). Modified NTH method for assessing effective friction angle of normally consolidated and overconsolidated clays from piezocone tests. Journal of Geotechnical and Geoenvironmental Engineering, 145(10), 04019067.

Li, H., Duan, M., Yang, X., Wang, R., & Ouyang, Z. (2025). Modified CPTU parameters and SBTn chart for predicting shear behavior of organic soils at large strains. Engineering Geology, 108273.

Ouyang, Z., & Mayne, P. W. (2018). Effective stress strength parameters of clays from DMT. Geotechnical Testing Journal, 41(5), 851-867.

Ouyang, Z., & Mayne, P. W. (2017). Effective friction angle of soft to firm clays from flat dilatometer. Proceedings of the Institution of Civil Engineers-Geotechnical Engineering, 170(2), 137-147.

Liang, Z., Malik, B. A., Jie, S., Duan, M., & Ouyang, Z. (2025, June). Investigation of Installation and Uplift Resistance of Suction Caisson Foundation Based on CPTU and DMT Methods. In ISOPE International Ocean and Polar Engineering Conference (pp. ISOPE-I). ISOPE.

Li, Y. Z., Zhang, J. P., Chen, Z. Y., Wang, H. C., Zhang, K. X., Hu, S. S., ... & Dudley, M. (2026, September). Growth and Characterization of High-Quality Thick Epitaxial 4H-SiC Wafers for

High Voltage Devices. In Defect and Diffusion Forum (Vol. 452, pp. 79-85). Trans Tech Publications Ltd.

Li, X., Wang, P., Li, G., & Zhang, Y. (2023). Design of a novel self-test-on-chip interface ASIC for capacitive accelerometers. IEEE Transactions on Circuits and Systems I: Regular Papers, 70(7), 2834-2843.

Xiong, S., Chen, T., Rupendra, A., Clement, C., Gasparri, E., & Lucchi, E. (2026). Embodied Carbon of Progressive Timber Integration in a 47-Storey Tropical High-Rise: A Singapore Public Housing Case Study. Building and Environment, 114910.

Yu, A., Pang, F., Yuan, Y., Huang, Y., Li, S., Yu, S., ... & Xia, L. (2023). Simultaneous current and vibration measurement based on interferometric fiber optic sensor. Optics & Laser Technology, 161, 109223.

Yu, A., Huang, Y., Li, S., Wang, Z., & Xia, L. (2023). All fiber optic current sensor based on phase-shift fiber loop ringdown structure. Optics Letters, 48(11), 2925-2928.

Zhang, S., Zhang, E., Cookson, J., Huang, P., & Yan, W. (2026). A hybrid XFEM-calibrated analytical framework for efficient fatigue crack growth prediction. International Journal of Fatigue, 109682.

Zhang, S., Huang, P., & Yan, W. (2024). A data-driven approach for railway in-train forces monitoring. Advanced Engineering Informatics, 59, 102258.

Lu, J., Xiong, H., Zhou, J., Lin, Z., & Feng, B. (2025, September). Collaborative Spatial and Channel Attention for Structural Vibration-based Gait Recognition. In 2025 IEEE International Joint Conference on Biometrics (IJCB) (pp. 1-11). IEEE.

Huang, S., Wang, S., Xu, C., Shi, Y., & Ye, F. (2019). Effect of grain gradation on the permeability characteristics of coarse-grained soil conditioned with foam for EPB shield tunneling. KSCE Journal of Civil Engineering, 23(11), 4662-4674.

Zhao, R., Tang, J., Zeng, W., Guo, Y., & Zhao, X. (2025). Towards human-like questioning: Knowledge base question generation with bias-corrected reinforcement learning from human feedback. Information Processing & Management, 62(3), 104044.

Zhao, R., Tang, J., Zeng, W., Chen, Z., & Zhao, X. (2024, October). Zero-shot knowledge graph question generation via multi-agent llms and small models synthesis. In Proceedings of the 33rd ACM International Conference on Information and Knowledge Management (pp. 3341-3351).

Li, Q., Ye, Q., Zhang, N., Zhang, W., & Hu, F. (2025). Digital-twin-enabled industrial IoT: Vision, framework, and future directions. IEEE Wireless Communications, 32(6), 173-181.

Li, S. (2025). Momentum, volume and investor sentiment study for us technology sector stocks—A hidden markov model based principal component analysis. PloS one, 20(9), e0331658.

Wang, S., Zhang, X., Wang, P., & Li, X. (2026). Design of Magnetic Sensor Array-Based PUFs for IoT Security. IEEE Transactions on Instrumentation and Measurement, 75, 1-9.

Zhang, B., Wang, S., Jiang, Y., Sui, D., Tu, Z., & Chu, D. (2025, July). Ask and Retrieve Knowledge: Towards Proactive Asking with Imperfect Information in Medical Multi-turn Dialogues. In Proceedings of the 48th International ACM SIGIR Conference on Research and Development in Information Retrieval (pp. 1055-1065).

Liu, X., Yu, Z., Yao, Y., Yang, K., Zeng, H., & Chen, C. P. (2026). A Comprehensive Survey of Cross-Modal Retrieval: Breaking Through Modal Barriers. ACM Computing Surveys.

Wang, J., Malawade, A. V., Zhou, J., Yu, S. Y., & Al Faruque, M. A. (2024, January). Rs2g: Data-driven scene-graph extraction and embedding for robust autonomous perception and scenario understanding. In 2024 IEEE/CVF Winter Conference on Applications of Computer Vision (WACV) (pp. 7478-7487). IEEE.

Yang, Z., Ji, W., & Wang, Z. (2024). Adaptive joint configuration optimization for collaborative inference in edge-cloud systems. Science China Information Sciences, 67(4), 149103.

Peng, Y., & Li, H. (2023). Benthic foraminiferal morphogroups at the end-Guadalupian extinction in eastern Sichuan Basin, China. Palaeogeography, Palaeoclimatology, Palaeoecology, 618, 111522.

Gao, X. L., & Wang, M. (2026). Enhancing cancer immunotherapy antibody discovery: Genetic algorithms and risk-aware protein modeling. Available at SSRN 6033537.

Syed, C., Yuan, K., Sui, M., Chambers, E., & Wilson, J. (2026). LLM-GRU-GAN: A Multi-Modal Adversarial Framework for Transactional Fraud Detection.

Jiao, F., Dong, X., Gong, Y., Chen, W., Wang, Y., & Zhang, S. L. (2018). Solid confirmation for the origin of the low-wave stray light in Raman spectra. Journal of Raman Spectroscopy, 49(12), 1968-1971.